Necking and fracking may explain stationary seismicity and full degassing in volcanic silicic spine extrusion

Liqing Jiao, Paul Tapponnier, Fidel Costa, Frédéric-Victor Donzé, Luc Scholtes, Benoit Taisne, Shengji Wei

Earth and Planetary Science Letters 503 (2018) 47–57

Contents lists available at ScienceDirect

Earth and Planetary Science Letters

www.elsevier.com/locate/epsl

Necking and fracking may explain stationary seismicity and full degassing in volcanic silicic spine extrusion

Liqing Jiao [a,*], Paul Tapponnier [a], Fidel Costa [a], Frédéric-Victor Donzé [b], Luc Scholtès [c], Benoit Taisne [a], Shengji Wei [a]

[a] Earth Observatory of Singapore, Nanyang Technological University, Singapore
[b] Université Grenoble Alpes, Institut des Sciences de la Terre, Grenoble, France
[c] Université de Lorraine, Lab. GeoRessources, Nancy, France

ARTICLE INFO

Article history:
Received 30 April 2018
Received in revised form 18 July 2018
Accepted 18 September 2018
Available online 1 October 2018
Editor: J.-P. Avouac

Keywords:
spine extrusion
volcanic seismicity
conduit necking
DEM modeling

ABSTRACT

Volcanic seismicity during silicic spine eruptions often involves recurrent excitation of similar sources at stationary depth just beneath the crater. The mechanics of volcanic spine extrusion may be compared to those of high-temperature, industrial metal working. We thus use slip-line field theory to assess stress, strain and faulting in ascending magma, which, although hot, behaves as a solid. Earthquake fault-plane solutions during the 09/2004–08/2005 eruptions of Mount St. Helens are generally consistent with shrinking of magma rising across a conduit "bottle-neck". Among 215 fault plane solutions, thrust and vertical fault planes prevail, with fewer normal or strike-slip faults. Constriction across the neck and vertical shear along the conduit walls thus predominate. Dynamic Discrete Element Modeling reproduces repetitive nucleation and growth of thrust faults within such a neck. The pressure drop across the neck's core (secondary tension) boosts crack opening and hence gas extraction. Such natural "fracking" could promote full magma degassing, contributing to the typically low explosivity of silicic spine extrusion.

1. Introduction

Volcanic seismicity (including low-frequency – 0.2 Hz to 10 Hz – events) is common during silicic dome and spine extrusions (Fig. 1). It spans a very broad spectrum that includes at its limits tremors and high frequency hybrid earthquakes (Chouet, 2003; Chouet and Matoza, 2013; McNutt, 2002), with signals varying from continuous to periodic. Hybrid and low-frequency events have been simply interpreted to have similar sources but different sizes (Horton et al., 2008). Many of these diverse events commonly occur in swarms, coevally with surface degassing (Pallister et al., 2013; Tuffen and Dingwell, 2005; Tuffen et al., 2008). The event sequences often include multiplets, which may repeat for minutes to weeks (Neuberg et al., 2006; Pallister et al., 2013). The source types span a very broad range. They include "drumbeat events", defined by Moran et al. (2008) as events that occur at remarkably constant intervals (see also Kendrick et al., 2014), low-frequency events, hybrid events and volcano-tectonic (VT) events (e.g., Moran et al., 2008). The regular occurrence, mostly in swarms, of many such events is thought to reflect the periodic excitation of repetitive, non-destructive sources (Lahr et al., 1994; Neuberg et al., 2006). Many hypocenters are commonly located at fairly constant depths beneath active domes (Lahr et al., 1994; Neuberg et al., 2006), (Fig. 2, Supplementary Fig. S1).

The origin and mechanisms of volcanic seismicity are not fully understood. It is generally thought that repetitive events result from faulting inside both the host-rock and the outer rims of the ascending magma (Chouet, 1996; Kendrick et al., 2014; Lahr et al., 1994; Neuberg et al., 2006; Pallister et al., 2013; Thomas and Neuberg, 2012; Voight et al., 1998). Yet, while boundary shear undoubtedly plays an important role, it does not suffice to account for the variable mechanisms of the earthquakes, and their frequent occurrence at fairly constant depths.

Understanding the mechanics of such volcanic earthquakes is important to elucidate eruptive processes and to assess related hazards. This, however, is a challenging goal because of the co-involvement of multiphase (gas/liquid/solid) thermal effects, large changes in physical properties (strength, viscosity, density), and magma flow geometry/kinematics (Chouet, 2003; Chouet and Matoza, 2013; Ramos et al., 1999). Crack opening along the conduit walls likely accounts for final gas escape around the crater rim (Jellinek and Bercovici, 2011), but not for the restricted depths of many events and full degassing of the magma interior. Abundant brittle-ductile deformation textures in silicic lavas im-

* Corresponding author.
E-mail address: jiao0019@e.ntu.edu.sg (L. Jiao).

https://doi.org/10.1016/j.epsl.2018.09.023

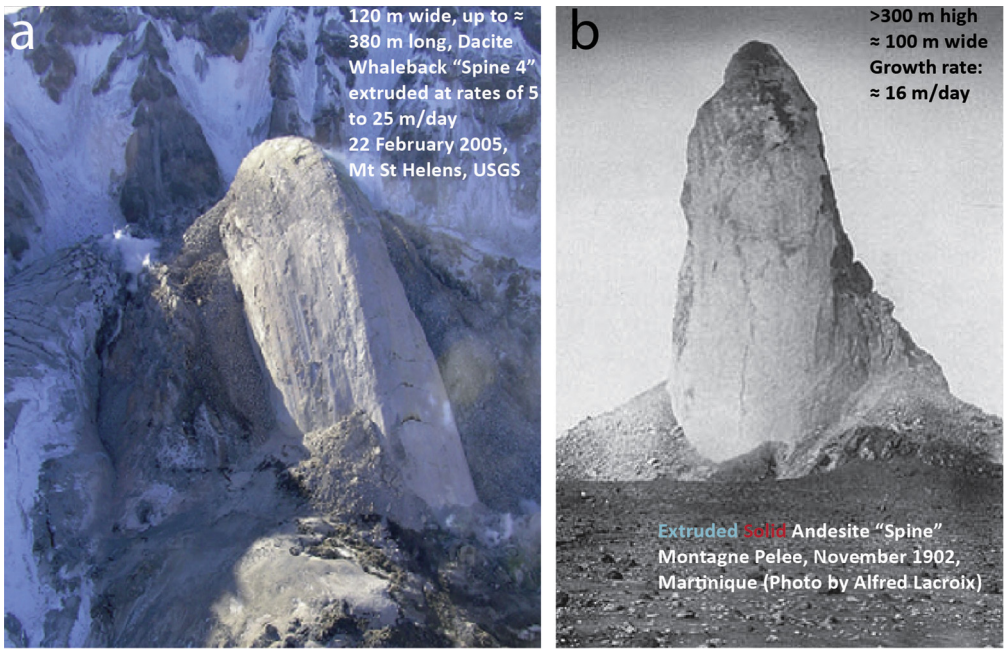

Fig. 1. Large silicic spines. (a) Emerging 2005 Mount St. Helens "whaleback" spine 4 (Pallister et al., 2013). (b) November 1902 solid, vertical spine of Montagne Pelée (Photograph by Alfred Lacroix).

ply fracturing/faulting within the magma itself (Green et al., 2006; Kendrick et al., 2014; Neuberg et al., 2006; Pallister et al., 2013; Thomas and Neuberg, 2012; Tuffen and Dingwell, 2005; Tuffen et al., 2008; Vargas-Bracamontes and Neuberg, 2012), which must thus behave as a solid. Studies at Soufrière Hills in Montserrat and Mount St. Helens suggest that this fracturing occurs primarily near the conduit wall, where the hot magma shears past cold host rock (Chouet and Matoza, 2013; Green et al., 2006; Heiken et al., 1988; Jousset et al., 2004; Kendrick et al., 2014; Pallister et al., 2013). In a particularly detailed study, Pallister et al. (2013) observed brittle faulting inside the edges of Spines 4 and 5 at Mount St. Helens (January to July 2005), and suggested that such brittle shear might start ∼1 km down along the conduit walls. Lateral faulting, however, is unlikely to be evenly distributed, for if it were, it would be difficult to account for the stationary depth of many of the largest earthquakes (Fig. 2, Supplementary Fig. S1). Increased lateral shear due to a narrowing conduit, as suggested by Thomas and Neuberg (2012), could trigger localized lateral faulting past the corresponding constriction, but such a geometrical change would not account for the decline or termination of such faulting farther upwards.

Nonetheless, changes in conduit width, which are likely as the magma ascends towards the surface, do suggest additional mechanisms that may simultaneously explain stationary – though recurrent – faulting as well as degassing within hot – though partly solid – magma, as it forces its way across a restricted path. Silicic spines are typically extruded obliquely or vertically as essentially coherent bodies that retain cohesion for days to weeks to lengths/elevations of hundreds of meters (e.g., Fig. 1) (Lacroix, 1904; Pallister et al., 2013). Though still hot, the extruded spine magmas thus likely behave as solids. Earthquakes, which require the transmission of shear stresses, only occur in solids. The depth at which silicic spines begin to behave mechanically as coherent solids is poorly known. However, upwards cooling/degassing likely fosters silicic magma crystallization enough that it may already contain up to ∼50% crystals at depths of 1 to 1.5 km below the crater. If so, such magma would behave as a weak solid, capable of shearing and cracking along faults, and hence generate earthquakes.

Large spine extrusion during silicic eruptions is fairly rare. Or rather, it has rarely been observed and described in detail. This may simply be because spines do not survive for long, as their magma rapidly disaggregates and collapses. Also, even large spines may remain hidden inside deep craters, as at Mount St. Helens, which would have hampered observation except possibly in the last few hundred years. Only a few would thus have been reported in this relatively short period of historical time. Finally, the conjunction of processes that we advocate in this paper may not be that common, as it requires both a permanent conduit bottleneck and an already solid ascending magma at the depth of that bottleneck. To our knowledge, the most outstanding historical cases of spine extrusion are those of Montagne Pelée in 1902 (when seismology was in infancy), and Mount St. Helens in 2004–2006. The set of instrumental seismic data during the latter is thus unique. Only a handful of other spine extrusion episodes, generally smaller or more inclined, are known to have occurred at Mt. Unzen (dacites, 1994, 2007, Japan), Santiaguito (andesites, 1958, 1967, Guatemala), Bezymianny (andesites, 1997, Kamchatka), and Chaiten (rhyolites, 2009, Chile). The most recent episodes at Unzen and Chaiten have been less completely studied seismically than Mount St. Helens. Our paper is thus primarily based on the Mount St. Helens dataset during the large spine extrusions of late 2004 and 2005.

Our goal here is not to account for all volcanic seismicity in general, but only for seismic events that are coeval with spine extrusion and occur at stationary depths. We show how the unique earthquake fault plane solutions dataset of Moran et al. (2008) at Mount St. Helens supports conduit width restriction as a major triggering mechanism, and how such a mechanism may be further validated by both theory (Backofen, 1972; Johnson et al., 1970) and discrete element modeling (Jiao et al., 2014).

2. Volcano structure and stationary eruptive seismicity

The structural settings of two typical and well-studied volcanic swarm sequences, at Soufrière Hills in the Caribbean and Mount St. Helens in Cascadia, are shown in Figs. 2a, b.

For the June 1997 Soufrière Hills swarms in Montserrat, most of the events occurred at depths between 1 and 1.3 km (Neuberg

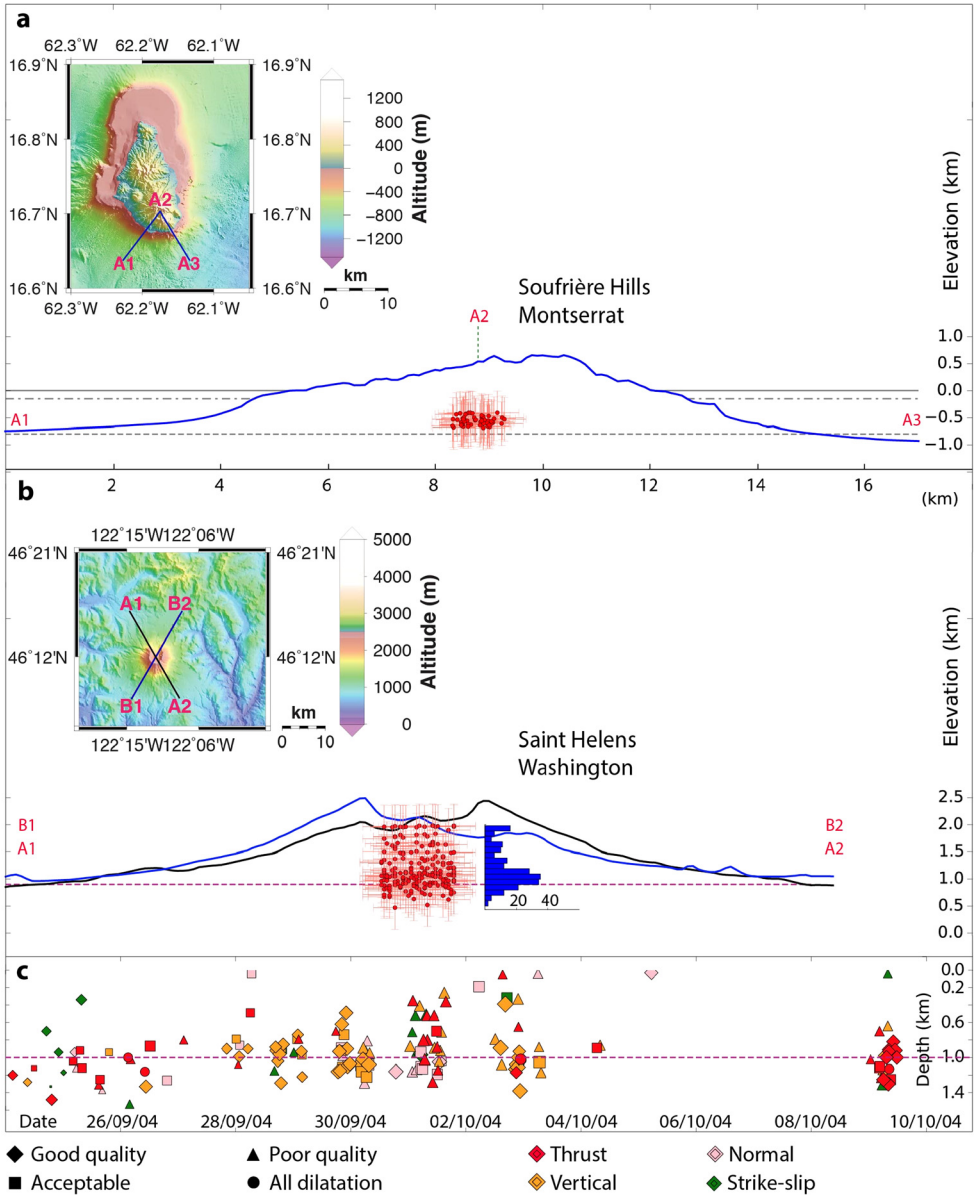

Fig. 2. Volcanic seismicity. (a) Top left: topography and bathymetry of Soufrière Hills and Montserrat. Bottom: Soufrière Hills' south-side topographic profiles A1–A2 and A2–A3, and location of 53 seismic swarm events (the solid red circles with thin error bars, June 1997, from Neuberg et al. (2006). Swarm events locations/depths under crater (A2) are extracted from Fig. 4d in Neuberg et al. (2006). The gray solid line is the present sea-level. The dotted-dashed line is the last glacial-maximum low-stand. The dashed line (∼1.3 km beneath crater) is the average see-floor depth around the volcano, projecting just beneath the seismic swarm). (b) Top left: topography of Mount St. Helens and adjacent Cascadia plateau, Washington. Bottom: topographic profiles A1–A2 and B1–B2 across the volcano, and 2D distribution of 216 volcanic seismic events (September 24, 2004 to August 27, 2005, the solid red symbols with thin error bars) from Moran et al. (2008). The histogram shows the statistics of depth distribution. The densest volcanic seismic swarm lies near the volcano baseline (the purple dashed line, ∼1.2 km below the crater). (c) 161 volcanic seismic events (September 24 to October 10, 2004). The symbol sizes reflect events' magnitudes (0.1 to 3.6). (For interpretation of the colors in the figure(s), the reader is referred to the web version of this article.)

et al., 2006), right below the ∼1 km wide crater center (station MBGA ∼1 km west of the dome, see Fig. 2 in Green and Neuberg, 2006). Within uncertainty, the hypocenters were located just above the projected depth of the seafloor upon which the volcano is built (Fig. 2a). The relatively complex geometry and topography of Soufrière Hills in map-view and cross-section (Fig. 2a) result from large-scale, oblique tectonic faulting across the northwest flank of the active dome, and from glacially driven sea-level change (Feuillet et al., 2010; Le Friant et al., 2009). While such 3D tectono-climatic processes might account for the small difference in average depth between the hypocenter cloud and the base of the volcanic edifice, they do not appear to have significantly affected the average localization of the events just beneath the extruding dome (Green and Neuberg, 2006; Neuberg et al., 2006).

For the thoroughly documented 09/2004–08/2005 eruptive sequence of Mount St. Helens (Figs. 1a and 2b, c, and Supplementary Fig. S1), a wealth of information is available (e.g., Horton et al., 2008; Moran et al., 2008; Qamar et al., 2008; Thelen et al., 2008). The eruption produced oblique, SE- to SW-wards extrusions of tilted, so-called "whaleback" spines, up to 460 m long (Fig. 1a). Volcanic seismicity swarms accompanied the extrusions, with most of the seismic events located at depths between 0.6 and 1.4 km beneath the crater floor, within a 1.2–2 km broad zone right underneath the center of the ∼2.3 km wide crater rim (Figs. 2b, c, Supplementary Fig. S1). Even with depth uncertainties of a few hundred meters, many earthquake hypocenters appeared to cluster near 1 km asl, a level corresponding roughly to the average elevation of the Cascadia plateau upon which the volcano is built (Figs. 2b, c, Supplementary Fig. S1).

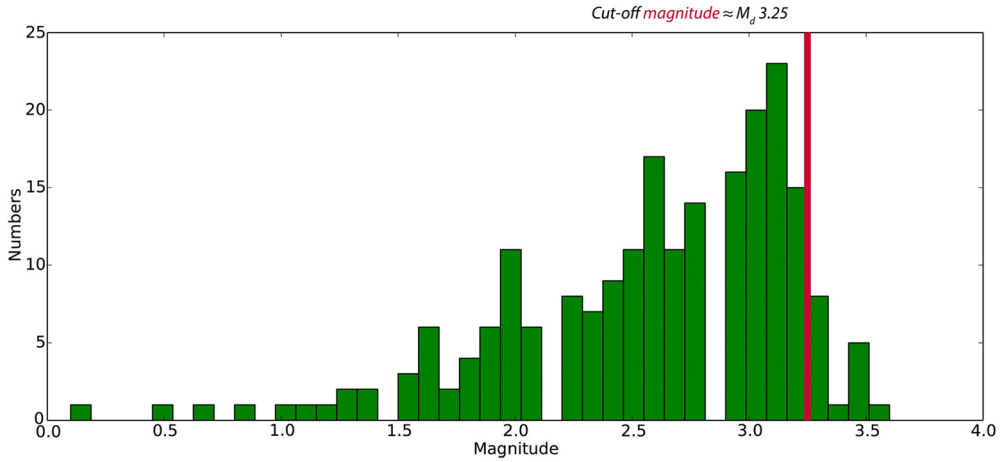

Fig. 3. 215 earthquake magnitudes distribution (binned). Note the regular increase in event abundance up to a sharp cut-off at $M_d \sim 3.25$.

Both examples illustrate a common feature of volcanic seismicity swarms (Neuberg et al., 2006; Thelen et al., 2008; Thomas and Neuberg, 2012): They often occur at roughly stationary depth beneath the center of the crater within which the spines/domes extrude, implying a causative link, likely controlled by crustal structure at that depth.

3. Earthquake mechanisms during Mount St. Helens spine extrusions

To date, the most quantitative dataset of volcanic seismicity during silicic-spine extrusion remains that of the 2004–2005 eruptions of Mount St. Helens. Based on waveform inversions results, Waite et al. (2008) and Matoza et al. (2015) prefer to explain a number of volcanic earthquake mechanisms by single-force sources, corresponding to volumetric oscillation of sub-horizontal cracks. Harrington and Brodsky (2007) and Moran et al. (2008), on the other hand, favor stick-slip (shear dislocation) to explain the corner frequencies and first motion polarities for most such earthquakes. Recent field and structural observations (Pallister et al., 2013) are also more consistent with stick-slip models, although they cannot rule out resonance of steam-filled fractures. This notwithstanding, stick-slip or shear dislocation may thus be taken to account for most of the seismic observations.

Even though more than a million seismic events were recorded at Mount St. Helens, only ~8,000 events could be located and many fewer (216), mostly the largest, yielded focal mechanisms linked with the spine ascent period (Moran et al., 2008). These latter events are thus the most useful to assess faulting at depth under the volcano during that period, and they are the largest set of focal mechanisms related to spine extrusion globally (Fig. 3 and Supplementary Fig. S2). Although other fault plane solutions have been obtained for generally smaller events (mostly M_d ~1) beneath the volcano's crater (Lehto et al., 2010), such events occurred at shallower depth (mostly <0.6 km) during the period from September 24 to 29 2004, and thus predated the first spine extrusion on October 11 2004 (Supplementary Fig. S3).

The coda duration magnitudes (M_d) of these events range between 0.5 and 3.5, with an abrupt cut-off at about M_d ~3.25 (Fig. 3, and Supplementary Fig. S4). This may be interpreted as reflecting the maximum possible source length, which would be on order of ~300 m. At a more detailed level, to determine the maximum rupture dimension (R) of volcanic seismic events during eruptions, we may use the following empirical equation, assuming a circular crack (Kanamori and Anderson, 1975):

$$R = \sqrt[3]{\frac{7 \cdot M_0}{16 \cdot \Delta\sigma}},$$

where M_0 is the seismic moment of the earthquake and $\Delta\sigma$ is the stress drop. Taking a stress drop of 0.5 MPa, as estimated for Mount St. Helens earthquakes by Harrington and Brodsky (2007), and a maximum M_w ($M_0 = 10^{9.1+1.5 \cdot M_w}$) of 3.0 results in a size of ~300 m. We use a slightly smaller M_w than the cutoff coda duration magnitude (M_d), which is often grossly overestimated (Qamar et al., 2008).

As is common in most volcanic seismicity studies, not all the 216 focal mechanisms in Moran et al. (2008) are simple double-couples, likely due to source complexity, and many suffer from sparse arrivals at the center of the focal sphere (Supplementary Figs. S2 and S5). Nevertheless, most of the solutions are of very good quality (more than nine clear first arrivals, compared to Roman et al. (2006) "high-quality" criteria of six clear first motion polarities). We thus use them at face value to clarify deformation mechanisms below the crater. The faulting patterns that emerge from this exceptional dataset are shown in Fig. 4 and Supplementary Fig. S6. The P/T (pressure/tension) axes orientations (equal-area projections) of individual focal mechanisms from the entire sequence suggest that the earthquakes may be separated into four distinct groups (Fig. 4).

The dominant mechanisms (99 events, 46% of the total, Fig. 4a) correspond to thrust faults. The thrust-slip directions are fairly uniformly distributed, but with second-order maxima oriented NNW and NNE (Supplementary Fig. S6a). The next most common solutions (68 events, 31%, Fig. 4b) correspond to vertical slip, plausibly along the conduit margins (e.g., Pallister et al., 2013; Thomas and Neuberg, 2012). At a more detailed level, the distribution of the nodal planes is also non-uniform, with asymmetry about a N-NNW striking direction (Fig. 4b and Supplementary Fig. S6b). The remaining two groups of mechanisms relate to less frequent events (about 25% of the total). They include normal (30 events, 14%, Fig. 4c) and strike-slip faults (19 events, 9%, Fig. 4d) events. The null vectors of the strike-slip mechanisms, including that of the deepest (8.2 km), likely tectonic, crustal event (# 216), are roughly aligned E–ESE (Fig. 4d and Supplementary Fig. S6d).

The deformation processes and structural settings of faults that could account for the earthquake mechanisms are sketched in Fig. 5. The dominant thrust mechanisms indicate horizontal, essentially radial shortening. Shrinking of the solid spine as it rises through a conduit "bottle-neck" (Fig. 5a) is the most plausible way to account for such shortening. The hot magma spine would be weaker than the colder surrounding host rocks, and thus faulting

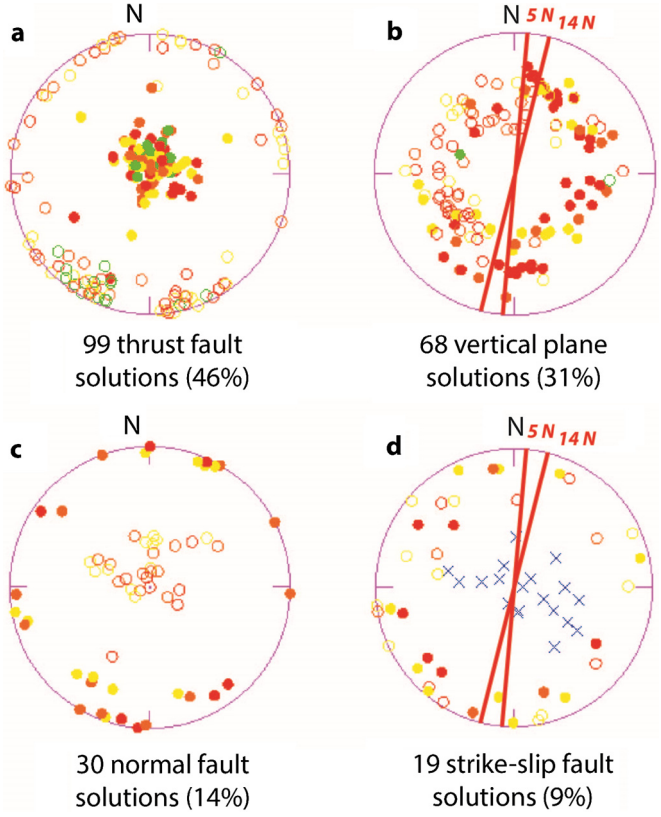

Fig. 4. Pressure (P) and tension (T) axes (the open and solid circles, respectively) plots of 216 seismic events, from fault-plane solutions of Moran et al. (2008). (a) 46% are thrust faults. (b) 31% are vertical faults. (c) 14% are normal faults. (d) 9% are strike-slip faults. The red dots are good-quality solutions; the orange dots are acceptable-quality solutions; the yellow dots are poor-quality solutions; the green dots are only tension first arrivals; the blue dots are null vectors. The red solid lines are maximum horizontal stress directions (containing P and T) from volcanic alignments south of Mount St. Helens (Indian Heaven, Three Fingered Jack, Two Sisters).

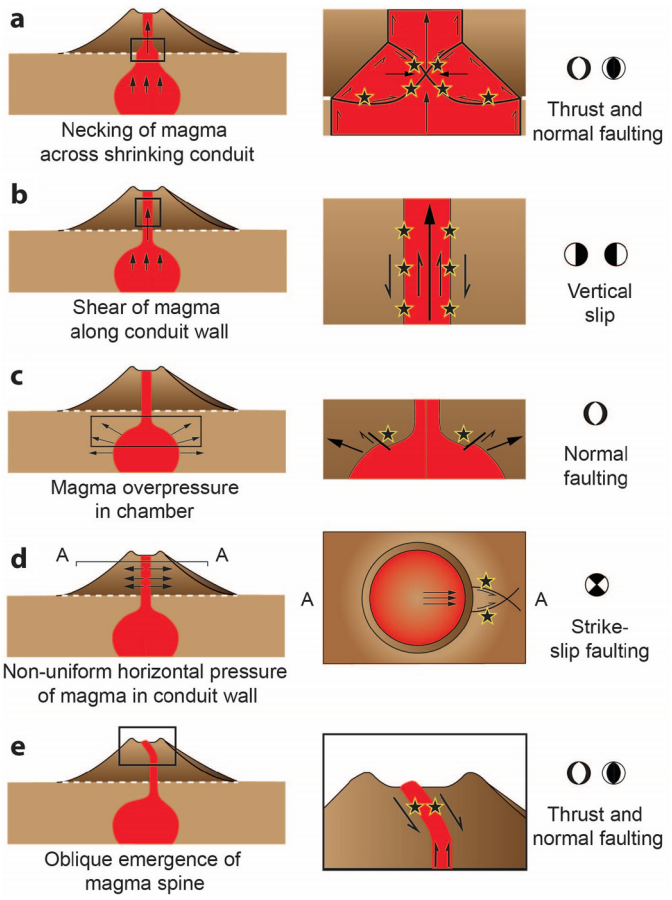

Fig. 5. Plausible volcanic seismicity sources. The small arrows below the volcano represent the pressure direction of ascending magma (left column). The square lines (left column) are locations of potential seismic sources, enlarged in the right column. The black stars (right column) are event epicenters. The half arrows (right column) show fault-slip directions. The beach balls on the right side show focal mechanisms of the following events: (a) Thrust faulting: spine constriction in the conduit neck. (b) Vertical slip of spine along the conduit wall. (c) Bedrock normal faulting due to collapse of the expanding magma chamber roof. (d) Bedrock strike-slip faulting due to non-uniform magma pressure in the conduit. (e) Normal/thrust faulting on conduit walls of shallow tilted spine.

would occur mostly inside rather than outside the spine. Conduit bottle-necks are likely to exist beneath the craters of both Mount St. Helens and Soufrière Hills at the base of the volcanic edifices (i.e., 1 to 1.5 km deep, Fig. 2 and 5a). At such depths, the spine would ascend across a fairly sharp geological contact between old, weathered, and young, stronger rocks (in Cascadia: Oligo-Miocene volcanic bedrock and Pleistocene dacites; in Montserrat: Tertiary pelagic sediments and Quaternary andesites), which ought to correspond to a taper from a wider to a narrower conduit. Across such a neck, the ascending magma (e.g., the 1902 spine of Montagne Pelée in Martinique, or the 2004–2005 spines of Mount St. Helens; Fig. 1) would have to contract horizontally and radially, while expanding vertically. Such shrinking/expansion would take place only at the passage across the neck, accounting for both the stationary depths of many events (Fig. 2), and for the apparent periodic excitation of repeatable, non-destructive sources (Lahr et al., 1994; Neuberg et al., 2006).

The second most frequent mechanisms (Fig. 4b and Supplementary Fig. S6b) are best interpreted to reflect vertical shear along the conduit walls during the upward ascent of the spine (Fig. 5b), as previously proposed (e.g., Neuberg et al., 2006; Thelen et al., 2008; Thomas and Neuberg, 2012) and recently validated by field observations (Pallister et al., 2013). The second-order asymmetry of the P and T axes distribution suggests that the shape of the conduit might be elliptical about a long axis trending ~N10 ± 5°E (Fig. 4b and Supplementary Fig. S6b). This direction is similar to those (N 5 to 14°N) of young volcanic alignments and eruptive dikes (Indian Heaven, Three Fingered Jack, Two Sisters) south of Mount St. Helens (Supplementary Fig. S7). It is thus consistent with the regional extension and minimum horizontal stress directions (N 95–104°E) in northern Cascadia (e.g., Zoback and Zoback, 1980).

The less frequent normal fault events (Fig. 4c and Supplementary Fig. S6c) may also be related to shear along the spine walls, but at various levels of the conduit. Magma rise on the inward-leaning sides of the neck would generate normal faulting (Fig. 5a). So would, at very shallow depth, shear on the downside of the inclined whaleback spines (Fig. 5e). At greater depths, lateral inflation of the magma reservoir due to increased magma pressure might trigger normal-fault collapse of the host rock in the reservoir roof (Fig. 5c), though the available 2004–2005 Mount St. Helens dataset is too shallow to test such a mechanism. The first two processes, however, may account for solutions shown in Figs. 2c and 4c and Supplementary Fig. S1c and S6c.

The least abundant strike-slip mechanisms (Fig. 4d and Supplementary Fig. S6d) may reflect local horizontal shortening and shear of the host rock outside the conduit due to non-uniform inflation of its wall by magma pressure (Fig. 5d). Although vertical planes containing the majority of the null vectors are roughly perpendicular to the ~N10 ± 5°E orientation, which coincides with the average surface extrusion direction of the whaleback spines (Supplementary Fig. S6d), the number of events is insufficient to

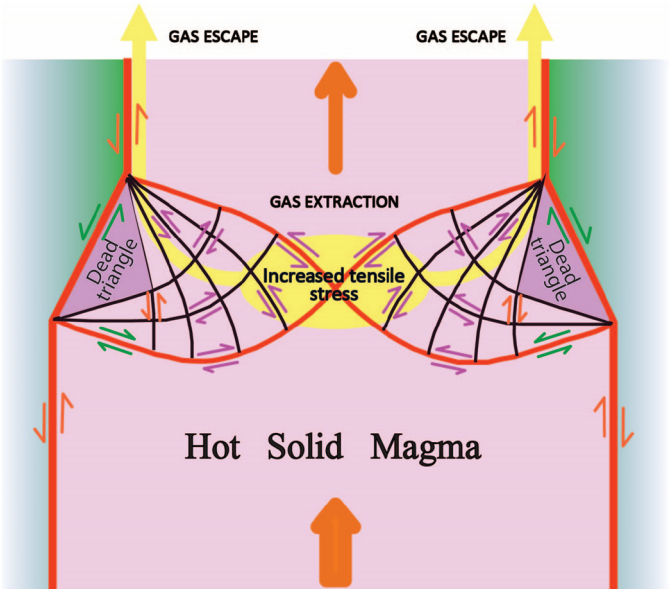

Fig. 6. The slip-line field for extrusion through a small reduction neck (after Johnson et al., 1970. The bold red lines are spine conduit walls. The large, full orange arrows show the spine ascent rate (slower in the lower conduit and faster in the upper conduit). The red/black thin curves are slip lines (the maximum shear stress trajectories). The purple triangles are "dead" zones. The purple, orange, and green double half-arrows represent thrust, vertical, and normal faults, respectively. The yellow elliptic zone at the center of the field demarcates the secondary tension area of fracking and gas extraction. The thick yellow lines show upward gas escape pathways.

assess their relationship with either in-situ stress or magma extrusion.

4. Stationary seismic necking, fracking and spine degassing

The deformation of a hot, solid volcanic spine ascending across a conduit restriction is mechanically identical to that documented during industrial shaping of hot metal rods (Backofen, 1972; McVeigh and Liu, 2006). Fig. 6 shows the analytical plane-strain slip-line field expected for extrusion through a frictionless, wedge-shaped neck (or die) of small reduction (Backofen, 1972; McVeigh and Liu, 2006). The orthogonal slip-lines are conjugate, maximum shear-stress trajectories, corresponding to the most likely newborn faults. Because their positions are fixed relative to the neck boundaries, they repeatedly nucleate as similar faults at these fixed positions within the moving spine. This simple mechanism can thus generate large numbers (swarms) of repeatable, nearly identical, stationary earthquakes, including multiplets, accounting for the apparent periodic excitation of repeatable, non-destructive sources noted in most studies (e.g., Neuberg et al., 2006). The high temperature of the ascending magma, close to the brittle/ductile transition, would be in keeping with the variable event types (drumbeat, low-frequency, hybrid, VT, etc.). Except for the tapered edges of the neck and the lateral sides of the basal slip-lines, which generate normal faulting (green arrows in Fig. 6), the majority of the slip lines correspond to thrust faults (purple arrows) that accommodate shrinking of the spine as it is forced through the narrower conduit neck (Fig. 6). Uniform, relatively weak friction along the spine walls would not significantly change such slip lines and faulting patterns (Backofen, 1972; McVeigh and Liu, 2006). Nor would a shift from plane to axisymmetric strain (Backofen, 1972; McVeigh and Liu, 2006). The overall fault distribution, geometry, and mechanisms predicted by the spine-necking model of Fig. 6 can thus account for the three main types (thrust, vertical slip, and normal), and relative abundance, of earthquake focal mechanisms documented at Mount St. Helens (Figs. 2, 4 and Supplementary Figs. S1c and S6).

There is additional, direct evidence for the existence of predominant thrust faults within the spine interiors at Mount St. Helens. Night-time infrared photographs of the largest emerging whaleback spine (Spine 3, November 29 2004, 10 m/day) (Schneider et al., 2008; Vallance et al., 2008) show, at the emerging base of that spine, several fault zones that crosscut its entire roof (Figs. 7a, b, and f). Because these faults act as conduits for hot gas escape, their detailed geometry and kinematics are brightly illuminated. None of them offsets the spine surface, which requires that they formed at depth, inside the spine, where the spine was still bounded by the conduit walls. That the intersections of the fault planes with the spine walls rise and curve back down from west to east (Figs. 7a, b, and f) indicates that they originated as south-dipping surfaces within the deep, originally vertical, ascending magma. As lightened by the hot escaping gases, the four clearly exposed, sub-parallel faults appear to be composed of right-stepping cracks (Figs. 1a, 7c, and d). This is consistent with thrust faulting inside the rising spine, before it was tilted southwards during emergence. Since limited by the total width of the spine, such thrust faults may only be at most ~300 m long (Fig. 7b), hence capable of generating earthquakes with maximum magnitudes of ~3, assuming a stress drop of 0.5 MPa (Harrington and Brodsky, 2007; Kanamori and Anderson, 1975), in keeping with those observed in the 2004–2005 sequence (Fig. 3). Additional support for this interpretation is provided by day-time photographs of Spines 3 and 5 (Cashman et al., 2008; Vallance et al., 2008). Large and small faults markedly oblique both to the steep edges and parallel directions of extrusion slickens and to the near horizontal basal emergence and other bathtub rings are clearly visible on the exposed sides of both spines (Supplementary Figs. S8a, b, c, adapted from Figs. 4a, b, and 27a of Cashman et al., 2008 and Vallance et al., 2008, respectively). Such faults clearly predate the distributed, parallel extrusion slickens that override them, and act as the main conduits of hot gas escape, which indicates that they extend deep into the spine.

In fact, the necking deformation process shown in Fig. 6 may account for the nearly complete degassing of silicic spine interiors, which limits their explosivity. Necks with relatively small reduction (i.e., moderate lateral shrinking relative to conduit width) produce fairly large confining-pressure drops inside the material that is forced across them (Hencky's law, (e.g., Backofen, 1972)). Such normal-stress drops ("secondary tension") increase towards the center of the neck, which commonly suffices to crack open weak, brittle material (e.g., McVeigh and Liu, 2006). Open cracks develop more densely at the center of the spine, in the maximum tension area where the symmetrical slip-lines meet (Fig. 6), and propagate on either side, providing continuous gas-escape paths towards the conduit edges. Secondary tension may thus be the most efficient mechanism to generate both swarms of internal cracks and open lateral faults, that is, connected, multiscale pathways for penetrative magma degassing within ascending solid spines. The whole process may be compared to industrial "fracking", which is widely used to retrieve captive hydrocarbons (notably gas) in tight reservoirs. Note that pervasive internal degassing would further accelerate crystallization and hence augment the brittleness of the magma. Loss of volatiles – notably water – has a huge effect on solidus temperatures of silicic magmas (Burnham, 1979; Cashman and Blundy, 2000). Hence, cracking and related degassing should have a runaway effect on spine crystallization and solidification.

Finally, note that the slip-line field model outlined in Fig. 6, which predicts the opening of sub-horizontal cracks, allowing for internal degassing in the central part of the spine where it ascends across the bottle-neck, would not be at odds with the existence of

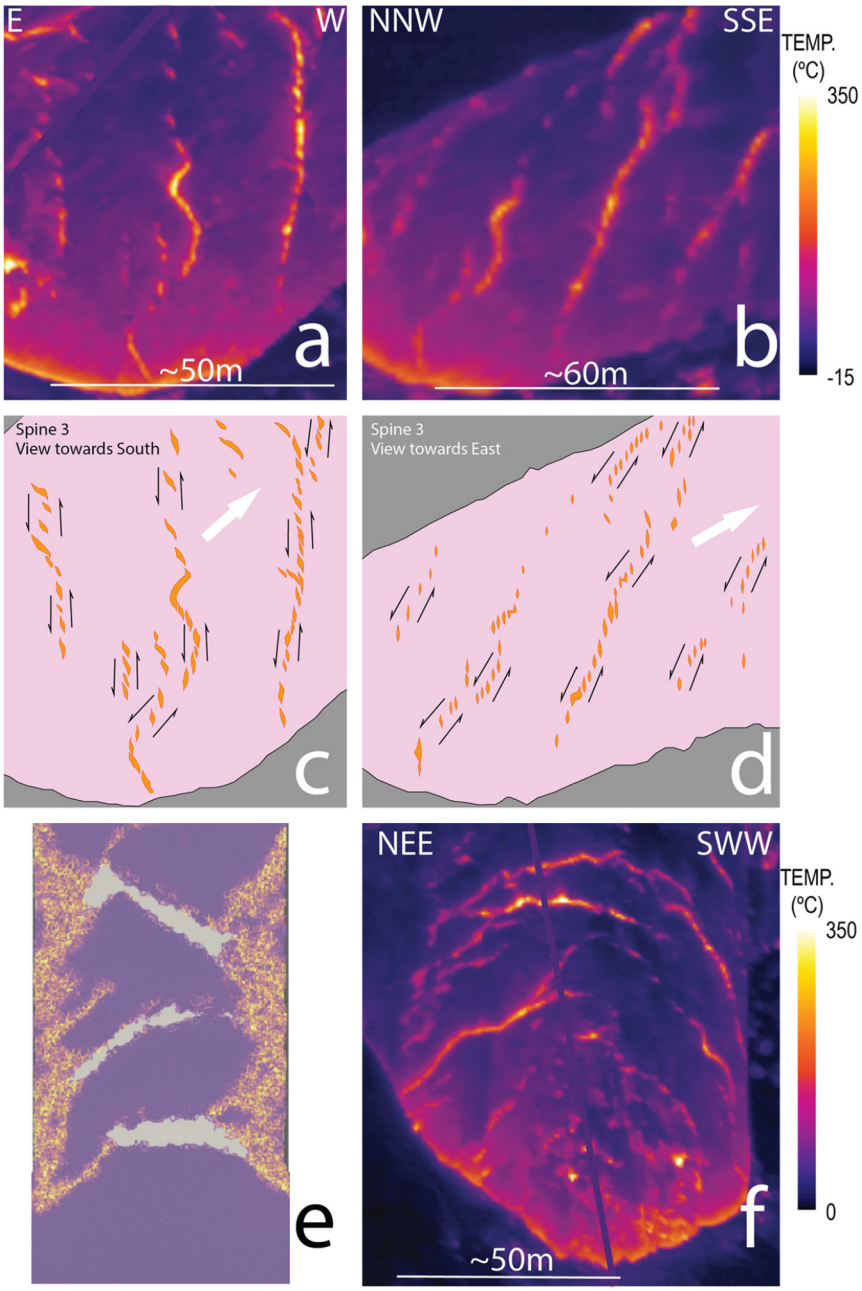

Fig. 7. Exhumed, deep thrust faults in the spine interior and a comparison of brittle crack opening in DEM and infrared image. (a), (b) Enlarged thermal-infrared images of Mount St. Helens spine 3 on November 29, 2004 (Schneider et al., 2008; Vallance et al., 2008), viewed towards south and east, respectively. The bright orange/yellow crack alignments are conduits of active gas-escape marking faults dipping into the spine. (c), (d) Interpretation of images (a)/(b): Cracks right-stepping and "en-echelons" arrangements (light-orange) are consistent with thrust faulting (the small half-arrows) inside the spine (pale-pink) when extrusion ascent (the large white arrows) is restored to vertical. (e) Zoomed modeling results (shear force, Fig. 10B). (f) Spine 3 faults on November 29, 2004, viewed from above – north.

single-force, oscillating, volumetric, sub-horizontal crack sources, as proposed by Waite et al. (2008) and Matoza et al. (2015).

5. Discrete Element Modeling of faulting across a spine neck

The detailed mechanisms of faulting within a weak solid spine ascending through a conduit restriction inside stronger bedrock at fixed depths may be further investigated with Discrete Element Modeling (DEM). In doing this, we follow previous attempts that have successfully investigated volcanic magma dynamics with the same approach (e.g. Bergantz et al., 2017). DEM was initially proposed by Cundall and Strack (1979) and further developed by Donzé et al. (1994), Hardy et al. (2009), and Scholtès and Donzé (2013). Here we use the YADE open DEM code (Šmilauer, 2015), developed specifically to explore discontinuous deformation, including strain-localization into shear-zones or faults, in various geo-materials.

We first calibrated the Von-Mises elasto-plastic model with a strain-softening component consistent with faulting in a brittle-plastic magma, using a simple square model under uniaxial, plane-strain compression (Fig. 8) (Scholtès and Donzé, 2013). The material is represented as an assembly of interacting particles. The overall behavior of that material is governed by the motion of its constitutive discrete elements, also called particles (ruled by Newton's second law). The computing cycle can be decomposed into four main steps related, respectively, to the determination

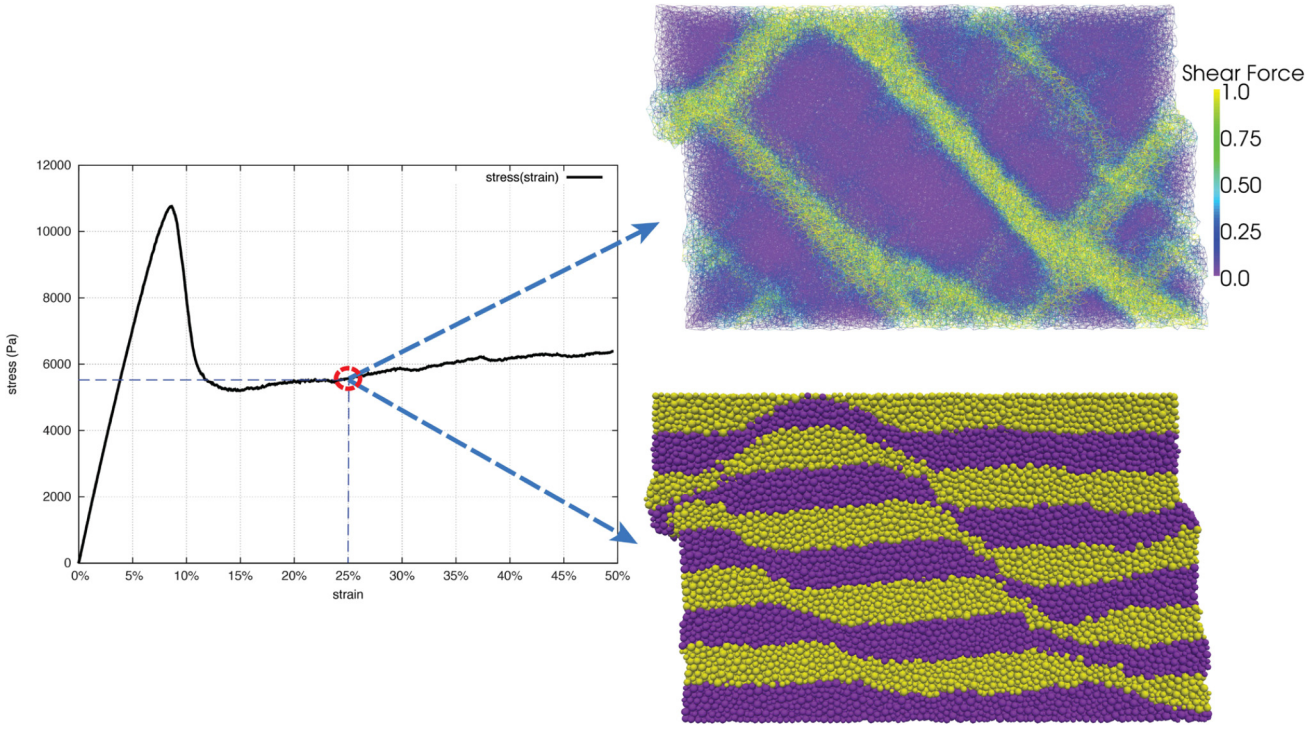

Fig. 8. The cubic, uniaxial compression test for modeling calibration. Left: The stress–strain curve of the model spine material. Top-right: Shear force localization at 25% strain. Bottom-right: Faulting and bulk deformation, outlined by alternately colored element layers, for 25% strain (see the references in the text for the modeling method, and algorithm/parametrization).

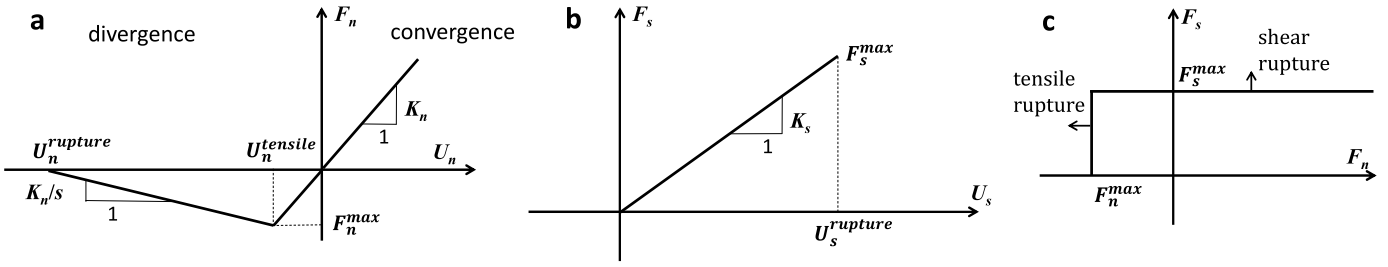

Fig. 9. The contact model used in the simulations: (a) normal behavior, (b) tangential behavior, and (c) failure envelope.

of the positions of the constitutive elements, the determination of their potential interaction, the computation of the forces applied to each of them according to predefined interaction laws, and the calculation of their updated positions through the integration of the equations of motion. The calculation cycle is repeated iteratively until the simulation stops (Scholtès and Donzé, 2013; Šmilauer, 2015). Because of the dynamic formulation of the method (explicit time-domain integration), a non-viscous damping is used to dissipate kinetic energy and facilitate convergence towards quasi-static equilibrium. This damping directly acts on the interaction forces – torques, respectively – in the equations of motion, so that the displacements are calculated from the damped force. This is a convenient numerical tool to ensure the convergence of the simulations (see Duriez et al., 2016 for details), but it needs to be used with caution (i.e., sensibility analysis) to prevent any bias. The behavior of the simulated medium is controlled by the behavior defined at the inter-particle scale. The inter-particle behavior of our DEM model can be decomposed into the normal and tangential directions of the contact plane. The normal contact model accounts for both divergence and convergence (Fig. 9).

In the convergence regime (compression of the contact/bond), the normal force F_n is computed as:

$$F_n = K_n \cdot U_n,$$

where U_n is the normal component of the relative displacement between particles A and B, and K_n the normal stiffness derived from the properties assigned to the particles, such that:

$$K_n = \frac{2 \cdot E_A \cdot R_A \cdot E_B \cdot R_B}{E_A \cdot R_A + E_B \cdot R_B},$$

where R_A and R_B are the radii of the particles and E_A and E_B, their respective elastic moduli, which are directly related to the bulk modulus of the simulated medium.

In the divergence regime (extension of the contact/bond), the normal force is computed with the same stiffness as that in the convergence regime. The inter-particle distance can increase up to $U_n^{tensile}$, for which the maximum admissible tensile force F_n^{max} is reached:

$$F_n^{max} = t \cdot A_{int},$$

with t the tensile strength of the interparticle bond and $A_{int} = \pi \cdot (\min(R_A, R_B))^2$ the interacting surface area between A and B.

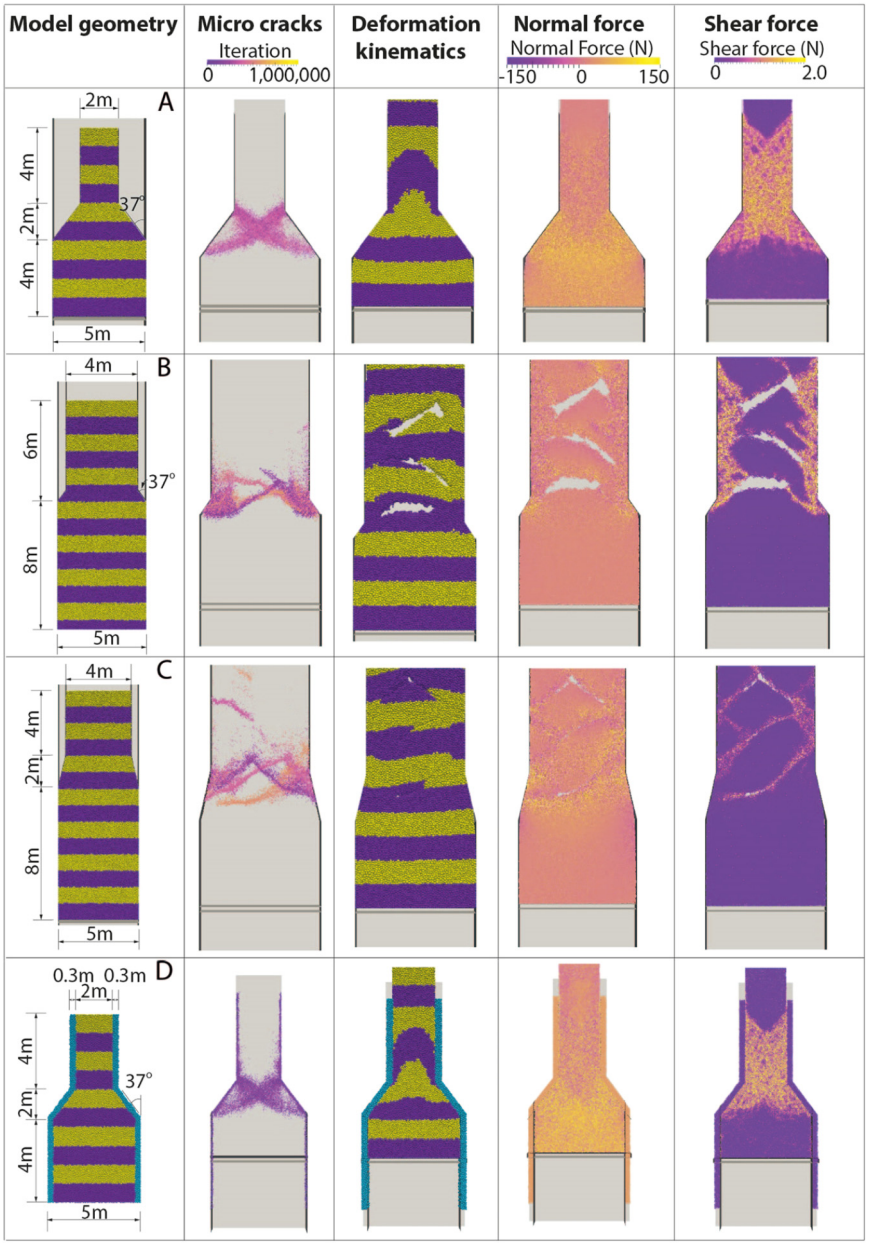

Fig. 10. Discrete element modeling of spine deformation (plane strain) across four different conduit necks. (A) Lower/upper conduit widths are 5 and 2 m, respectively. The neck length is 2 m. The reduction angle is 37°. (B) Lower/upper conduit widths are 5 and 4 m, respectively. The reduction angle is 37°. (C) Lower/upper conduit widths are 5 and 4 m, respectively. The neck length is 2 m. (D) The neck size and geometry is the same as in (A), with friction along the conduit walls. Boundary conditions: The top of the conduit is open, and the lateral walls are rigid. The rate of the rigid plate rise at the base of the spine is 10^{-3} m/s. The conduit walls are frictionless except in and above the neck in (D). For normal force (N), compression/tension are positive/negative, respectively. Physical parameters: Young's modulus is $3 * 10^5$ Pa; the a value (related to Poisson's ratio) is 0.004; the Friction angle is 0; the tensile strength is $1 * 10^3$ Pa; Cohesion is $1 * 10^3$ Pa; K (the coordination number, which controls brittleness) is 10; and S (the weakening gradient) is 10; total healing.

When F_n^{max} is reached, the force is not set to zero immediately as is usually the case in brittle rock modeling (e.g., Scholtès and Donzé, 2013). Instead, F_n gradually decreases, following the softening behavior at the particle scale, between $U_n^{tensile} < U_n < U_n^{rupture}$, according to:

$$F_n = F_n^{max} - \frac{K_n}{s}\left(U_n - U_n^{tensile}\right),$$

where s is a weakening coefficient that needs to be defined. If the inter-particle distance continues to increase, the inter-particle bond breaks when $U_n > U_n^{rupture}$ and all forces are set to zero. A crack is then defined at the location of the bond breakage.

As in classic DEM formulations (Hart et al., 1988), the tangential force F_s at the current time step t is computed incrementally as:

$$F_s^{(t)} = F_s^{(t-\Delta t)} + K_s \cdot \Delta U_s,$$

with $F_s^{(t-\Delta t)}$ the force computed at the previous time step, ΔU_s the incremental tangential displacement between A and B, and K_s the tangential stiffness, defined as $K_S = a \cdot K_n$ with a, a coefficient related to the Poisson's ratio of the simulated medium.

As for the normal force, a maximum admissible tangential force F_s^{max} is defined as:

$$F_s^{max} = c \cdot A_{int},$$

with c the inter-particle cohesion (Fig. 9). Once the tangential force reaches this limit, the inter-particle bond breaks and the forces are set to zero. A crack is then defined at the location of the bond breakage.

One additional parameter is introduced to enable healing of newly created inter-particle contacts. Bonds are thus created when new inter-particle contacts are detected during the simulation. These bonds have the same strength as the initial ones. This is a way to model the healing processes that eventually take place along faults. It permits to control the dilatancy of the medium undergoing failure.

Using the algorithm above, the uniaxial compression test shows a strain softening behavior. Strain softening (Fig. 8 left) is associated with shear localization that leads to faulting (Fig. 8 top and bottom right). Under plane-strain conditions, with simple neck geometries and zero/low friction along the conduit-walls, the evolving stress and strain fields were computed and the nucleation and growth of faults in and above the conduit neck were accurately monitored. The supplementary animations 1 and 2 illustrate the progressive deformation and fault/crack development, as well as the changes in strain and normal/shear stresses in the ascending magma. As shown in Figs. 7e and f, there is a particularly striking correspondence between the faults and cracks generated in our DEM models and those observed in the emergent Mount St. Helens 2004 spine 3.

In all the models, the magma ascending past the shrinking conduit is fractured by constriction, with thrust faulting along the maximum shear stress trajectories (cracks, shear force, Fig. 10), in keeping with slip-line field theoretical predictions (Fig. 6). The thrusts are repeatedly renewed in stationary position within the moving magma. For reductions in conduit width of less than ~20% over similarly short lengths (Figs. 10b, and c), the hydrostatic pressure (normal force) drops in the middle of the conduit, past the neck (Supplementary Animation 1), as required by the upward increase in extrusion rate. This "secondary tension" (Backofen, 1972; Johnson et al., 1970) drives the vertical opening of shallow-dipping/horizontal cracks (Supplementary Animation 2). In the natural environment, such cracks (Figs. 7e and f) would readily extract gas from the magma (natural "fracking"), and might also resonate seismically. Even though the DEM approach we use here was set up for 2D deformation (plane strain), none of the main results would be altered by cylindrical geometry. Similarly, introducing plausibly small friction coefficient values along the conduit walls would have only minor effects on faulting inside the spine (see deformation kinematics and normal force, Fig. 10d). Note that even though our model does not explicitly account for gas extraction, the strong degassing generally observed along spine conduit walls, which implies efficient, steady fluid escape, implies reduced interface contact, hence low friction.

6. Conclusions

Many of the earthquakes recorded during Mount St. Helens 2004–2005 eruptions occurred right below the crater, at shallow, roughly stationary depths (~1 ± 0.4 km). They show two principal types of focal-mechanisms (thrust and vertical slip). In addition to abundant events reflecting slip along the conduit walls (e.g., Pallister et al., 2013; Thomas and Neuberg, 2012), the most frequent earthquakes (nearly 50%) imply thrust faulting. This pattern may be typical of volcanic seismicity during silicic spine ascent in general.

We propose that the dominant seismic events are repeatedly triggered at fixed locations inside the rising magma, which behaves as a solid compressed laterally and stretched vertically while passing across a conduit bottleneck. The vertical tensile stresses (secondary tension) generated in the magma by such "necking" cause the opening of shallow-dipping, penetrative cracks within the spine, allowing for full, pervasive gas extraction ("fracking"). These cracks efficiently channel gas flow all the way across the spine, towards vertical ascent/escape along the conduit walls. Fracking due to necking can thus explain the remarkably effective, penetrative loss of volatiles that contributes to fostering magma solidification in ascending spines. Additionally, fluid/gas infilling of opening cracks might account for low frequency seismic resonance. Simple dynamic modeling (DEM) validates the formation of thrust faults and open cracks within a conduit neck of small reduction, as often observed during industrial shaping of hot metals, and predicted by slip-line field theory.

The interrelated mechanisms we describe here are triggered by simple, hence probably common, changes of conduit geometry that may be readily related to local, shallow crustal structure and geological history. Besides illuminating the focal mechanisms of specific volcanic seismic events, necking is consistent with the existence of a localized zone of renewable, stationary faulting inside the conduit, as generally observed beneath craters, rather than mostly along conduit walls, which ought to correspond with hollow epicenter distributions. Natural fracking provides a superior mechanism for extracting gas out of solid magma, and hence contributes to elucidate the hitherto puzzling non-explosive nature of silicic spine ascent. Further testing of such a dual necking/fracking process should be a prime target in future instrumental studies of spine eruptions.

Acknowledgments

The research was entirely funded by the Earth Observatory of Singapore (EOS, NTU, Singapore; M4430233.B50.706022). Professor Paul Tapponnier is grateful to Dr. Chris Newhall for the initial scientific exchanges that inspired the development of this project. Dr. Liqing Jiao started this project for her Ph.D.-qualifying examination under the supervision of Associate Professor Fidel Costa. We thank Dr. Corentin Caudron for fruitful discussion about volcanic seismicity. We thank two anonymous reviewers for constructive comments. We also thank Yves Descatoire for his help in drafting Fig. 3. This work is Earth Observatory of Singapore contribution No. 207. This research is supported by the National Research Foundation Singapore and the Ministry of Education - Singapore under the Research Centres of Excellence initiative.

Appendix A. Supplementary material

Supplementary material related to this article can be found online at https://doi.org/10.1016/j.epsl.2018.09.023.

References

Backofen, W.A., 1972. Deformation Processing. Addison–Wesley Pub. Co.
Bergantz, G.W., Schleicher, J.M., Burgisser, A., 2017. On the kinematics and dynamics of crystal-rich systems. J. Geophys. Res., Solid Earth 122, 6131–6159.
Burnham, C.W., 1979. The importance of volatile constituents. In: The Evolution of the Igneous Rocks, vol. 439, p. 82.
Cashman, K.V., Blundy, J., 2000. Degassing and crystallization of ascending andesite and dacite. Philos. Trans. R. Soc. Lond. A, Math. Phys. Eng. Sci. 358, 1487–1513.
Cashman, K.V., Thornber, C.R., Pallister, J.S., 2008. From Dome to Dust: Shallow Crystallization and Fragmentation of Conduit Magma During the 2004–2006 Dome Extrusion of Mount St. Helens, Washington. US Geological Survey Professional Paper, pp. 387–413.
Chouet, B., 1996. Long-period volcano seismicity: its source and use in eruption forecasting. Nature 380, 309–316.
Chouet, B., 2003. Volcano seismology. Pure Appl. Geophys. 160, 739–788.
Chouet, B., Matoza, R., 2013. A multi-decadal view of seismic methods for detecting precursors of magma movement and eruption. J. Volcanol. Geotherm. Res. 252, 108–175.
Cundall, P.A., Strack, O.D.L., 1979. Discrete numerical model for granular assemblies. Geotechnique 29, 47–65.
Donzé, F., Mora, P., Magnier, S.A., 1994. Numerical simulation of faults and shear zones. Geophys. J. Int. 116, 46–52.

Duriez, J., Scholtès, L., Donzé, F.-V., 2016. Micromechanics of wing crack propagation for different flaw properties. Eng. Fract. Mech. 153, 378–398.
Feuillet, N., Leclerc, F., Tapponnier, P., Beauducel, F., Boudon, G., Le Friant, A., Deplus, C., Lebrun, J.F., Nercessian, A., Saurel, J.M., 2010. Active faulting induced by slip partitioning in Montserrat and link with volcanic activity: new insights from the 2009 GWADASEIS marine cruise data. Geophys. Res. Lett. 37.
Green, D.N., Neuberg, J., 2006. Waveform classification of volcanic low-frequency earthquake swarms and its implication at Soufrière Hills Volcano, Montserrat. J. Volcanol. Geotherm. Res. 153, 51–63.
Green, D.N., Neuberg, J., Cayol, V., 2006. Shear stress along the conduit wall as a plausible source of tilt at Soufriere Hills volcano, Montserrat. Geophys. Res. Lett. 33.
Hardy, S., McClay, K., Munoz, J.A., 2009. Deformation and fault activity in space and time in high-resolution numerical models of doubly vergent thrust wedges. Mar. Pet. Geol. 26, 232–248.
Harrington, R.M., Brodsky, E.E., 2007. Volcanic hybrid earthquakes that are brittle-failure events. Geophys. Res. Lett. 34.
Hart, R., Cundall, P., Lemos, J., 1988. Formulation of a three-dimensional distinct element model – part II: mechanical calculations for motion and interaction of a system composed of many polyhedral blocks. Int. J. Rock Mech. Min. Sci. Geomech. Abstr., 117–125.
Heiken, G., Wohletz, K., Eichelberger, J., 1988. Fracture fillings and intrusive pyroclasts, Inyo Domes, California. J. Geophys. Res. 93, 4335–4350.
Horton, S., Norris, R.D., Moran, S., 2008. Broadband characteristics of earthquakes recorded during a dome-building eruption at Mount St. Helens, Washington, between October 2004 and May 2005. In: A Volcano Rekindled: The Renewed Eruption of Mount St. Helens 2006, pp. 97–110.
Jellinek, A.M., Bercovici, D., 2011. Seismic tremors and magma wagging during explosive volcanism. Nature 470, 522–525.
Jiao, L., Tapponnier, P., Costa, F., Taisne, B., Donzé, F., Scholtès, L., 2014. Discrete element modeling of spine extrusion, and origin of volcanic low-frequency seismicity. In: The 11th Annual Meeting of the Asia Oceania Geosciences Society. AOGS 2014, Sapporo, Japan.
Johnson, W., Sowerby, R., Haddow, J.B., 1970. Plane Strain Slip-Line Fields: Theory and Bibliography.
Jousset, P., Neuberg, J., Jolly, A., 2004. Modelling low-frequency volcanic earthquakes in a viscoelastic medium with topography. Geophys. J. Int. 159, 776–802.
Kanamori, H., Anderson, D.L., 1975. Theoretical basis of some empirical relations in seismology. Bull. Seismol. Soc. Am. 65, 1073–1095.
Kendrick, J., Lavallée, Y., Hirose, T., Di Toro, G., Hornby, A., De Angelis, S., Dingwell, D., 2014. Volcanic drumbeat seismicity caused by stick-slip motion and magmatic frictional melting. Nat. Geosci.
Lacroix, A., 1904. La Montagne Pelee et ses eruptions. Masson et Cie, Paris.
Lahr, J.C., Chouet, B.A., Stephens, C.D., Power, J.A., Page, R.A., 1994. Earthquake classification, location, and error analysis in a volcanic environment – implications for the magmatic system of the 1989–1990 eruptions at Redoubt volcano, Alaska. J. Volcanol. Geotherm. Res. 62, 137–151.
Le Friant, A., Deplus, C., Boudon, G., Sparks, R., Trofimovs, J., Talling, P., 2009. Submarine deposition of volcaniclastic material from the 1995–2005 eruptions of Soufrière Hills volcano, Montserrat. J. Geol. Soc. 166, 171–182.
Lehto, H.L., Roman, D.C., Moran, S.C., 2010. Temporal changes in stress preceding the 2004–2008 eruption of Mount St. Helens, Washington. J. Volcanol. Geotherm. Res. 198, 129–142.
Matoza, R.S., Chouet, B.A., Dawson, P.B., Shearer, P.M., Haney, M.M., Waite, G.P., Moran, S.C., Mikesell, T.D., 2015. Source mechanism of small long-period events at Mount St. Helens in July 2005 using template matching, phase-weighted stacking, and full-waveform inversion. J. Geophys. Res., Solid Earth 120, 6351–6364.
McNutt, S.R., 2002. Volcano seismology and monitoring for eruptions. Int. Geophys. Ser. 81, 383–406.
McVeigh, C., Liu, W.K., 2006. Prediction of central bursting during axisymmetric cold extrusion of a metal alloy containing particles. Int. J. Solids Struct. 43, 3087–3105.
Moran, S.C., Malone, S.D., Qamar, A.I., Thelen, W.A., Wright, A.K., Caplan-Auerbach, J., 2008. Seismicity Associated with Renewed Dome Building at Mount St. Helens, 2004–2005. US Geological Survey Professional Paper, pp. 27–60.
Neuberg, J.W., Tuffen, H., Collier, L., Green, D., Powell, T., Dingwell, D., 2006. The trigger mechanism of low-frequency earthquakes on Montserrat. J. Volcanol. Geotherm. Res. 153, 37–50.
Pallister, J.S., Cashman, K.V., Hagstrum, J.T., Beeler, N.M., Moran, S.C., Denlinger, R.P., 2013. Faulting within the Mount St. Helens conduit and implications for volcanic earthquakes. Geol. Soc. Am. Bull. 125, 359–376.
Qamar, A.I., Malone, S.D., Moran, S.C., Steele, W.P., Thelen, W.A., 2008. Near-Real-Time Information Products for Mount St. Helens-Tracking the Ongoing Eruption. US Geological Survey Professional Paper, pp. 61–70.
Ramos, E.G., Hamburger, M.W., Pavlis, G.L., Laguerta, E.P., 1999. The low-frequency earthquake swarms at Mount Pinatubo, Philippines: implications for magma dynamics. J. Volcanol. Geotherm. Res. 92, 295–320.
Roman, D., Neuberg, J., Luckett, R., 2006. Assessing the likelihood of volcanic eruption through analysis of volcanotectonic earthquake fault–plane solutions. Earth Planet. Sci. Lett. 248, 244–252.
Schneider, D.J., Vallance, J.W., Wessels, R.L., Logan, M., Ramsey, M.S., 2008. Use of thermal infrared imaging for monitoring renewed dome growth at Mount St. Helens, 2004. In: A Volcano Rekindled, 2004–2006.
Scholtès, L., Donzé, F.V., 2013. A DEM model for soft and hard rocks: role of grain interlocking on strength. J. Mech. Phys. Solids 61, 352–369.
Šmilauer, V., 2015. Yade Documentation, 2nd ed. The Yade Project.
Thelen, W.A., Crosson, R.S., Creager, K.C., 2008. Absolute and Relative Locations of Earthquakes at Mount St. Helens, Washington, Using Continuous Data: Implications for Magmatic Processes. US Geological Survey Professional Paper, pp. 71–95.
Thomas, M.E., Neuberg, J., 2012. What makes a volcano tick – a first explanation of deep multiple seismic sources in ascending magma. Geology 40, 351–354.
Tuffen, H., Dingwell, D., 2005. Fault textures in volcanic conduits: evidence for seismic trigger mechanisms during silicic eruptions. Bull. Volcanol. 67, 370–387.
Tuffen, H., Smith, R., Sammonds, P.R., 2008. Evidence for seismogenic fracture of silicic magma. Nature 453, 511–514.
Vallance, J.W., Schneider, D.J., Schilling, S.P., 2008. Growth of the 2004–2006 Lava-Dome Complex at Mount St. Helens, Washington. US Geological Survey Professional Paper, pp. 169–208.
Vargas-Bracamontes, D.M., Neuberg, J.W., 2012. Interaction between regional and magma-induced stresses and their impact on volcano-tectonic seismicity. J. Volcanol. Geotherm. Res. 243, 91–96.
Voight, B., Hoblitt, R.P., Clarke, A.B., Lockhart, A.B., Miller, A.D., Lynch, L., McMahon, J., 1998. Remarkable cyclic ground deformation monitored in real-time on Montserrat, and its use in eruption forecasting. Geophys. Res. Lett. 25, 3405–3408.
Waite, G.P., Chouet, B.A., Dawson, P.B., 2008. Eruption dynamics at Mount St. Helens imaged from broadband seismic waveforms: interaction of the shallow magmatic and hydrothermal systems. J. Geophys. Res., Solid Earth (1978–2012), 113.
Zoback, M.L., Zoback, M., 1980. State of stress in the conterminous United States. J. Geophys. Res., Solid Earth 85, 6113–6156.